Title

Evapotranspiration across plant types and geomorphological units in polygonal Arctic tundra

Authors

Raz-Yaseef, Naama
Young-Robertson, Jessica
Rahn, Thom
et al.

Publication Date

2017-10-01

DOI

10.1016/j.jhydrol.2017.08.036

Peer reviewed

Journal of Hydrology 553 (2017) 816–825

Contents lists available at ScienceDirect

Journal of Hydrology

journal homepage: www.elsevier.com/locate/jhydrol

Research papers

Evapotranspiration across plant types and geomorphological units in polygonal Arctic tundra

Naama Raz-Yaseef [a,*], Jessica Young-Robertson [b], Thom Rahn [c], Victoria Sloan [d], Brent Newman [c], Cathy Wilson [c], Stan D. Wullschleger [e], Margaret S. Torn [a,f,*]

[a] Lawrence Berkeley National Laboratory, Berkeley, CA, USA
[b] University of Alaska Fairbanks, Fairbanks, AK, USA
[c] Los Alamos National Laboratory, Los Alamos, NM, USA
[d] University of Bristol, Bristol, UK
[e] Oak Ridge National Laboratory, Oak Ridge, TN, USA
[f] University of California, Berkeley, CA, USA

ARTICLE INFO

Article history:
Received 26 October 2016
Received in revised form 17 August 2017
Accepted 22 August 2017
Available online 31 August 2017
This manuscript was handled by Tim R. McVicar, Editor-in-Chief, with the assistance of Joshua Larsen, Associate Editor

Keywords:
Arctic tundra
Evapotranspiration
Greenhouse gases
Moss
Polygon structure

ABSTRACT

Coastal tundra ecosystems are relatively flat, and yet display large spatial variability in ecosystem traits. The microtopographical differences in polygonal geomorphology produce heterogeneity in permafrost depth, soil temperature, soil moisture, soil geochemistry, and plant distribution. Few measurements have been made, however, of how water fluxes vary across polygonal tundra plant types, limiting our ability to understand and model these ecosystems. Our objective was to investigate how plant distribution and geomorphological location affect actual evapotranspiration (ET). These effects are especially critical in light of the rapid change polygonal tundra systems are experiencing with Arctic warming. At a field site near Barrow, Alaska, USA, we investigated the relationships between ET and plant cover in 2014 and 2015. ET was measured at a range of spatial and temporal scales using: (1) An eddy covariance flux tower for continuous landscape-scale monitoring; (2) An automated clear surface chamber over dry vegetation in a fixed location for continuous plot-scale monitoring; and (3) Manual measurements with a clear portable chamber in approximately 60 locations across the landscape. We found that variation in environmental conditions and plant community composition, driven by microtopographical features, has significant influence on ET. Among plant types, ET from moss-covered and inundated areas was more than twice that from other plant types. ET from troughs and low polygonal centers was significantly higher than from high polygonal centers. ET varied seasonally, with peak fluxes of 0.14 mm h^{-1} in July. Despite 24 hours of daylight in summer, diurnal fluctuations in incoming solar radiation and plant processes produced a diurnal cycle in ET. Combining the patterns we observed with projections for the impact of permafrost degradation on polygonal structure suggests that microtopographic changes associated with permafrost thaw have the potential to alter tundra ecosystem ET.

Published by Elsevier B.V.

1. Introduction

Arctic tundra biomes account for nearly 10% of the Earth's surface (Schlesinger and Bernhardt, 2013) and are the most common land cover north of the Arctic Circle. Arctic climate has warmed significantly over the last several decades, at a rate that is approximately twice that of lower latitudes ('Arctic amplification'; Spielhagen et al., 2011, Screen and Francis, 2016). Warming temperatures have led to considerable changes in Arctic regions, including permafrost thaw and degradation (Jorgenson et al., 2006; Liljedahl et al., 2016), soil carbon release (Schuur et al., 2008, Strauss et al., 2013, Schädel et al., 2016), and changes in vegetation distribution and productivity ('Arctic greening'; Tape et al., 2006, Goetz et al., 2011). Observed trends of near-surface wind speeds show an increase for most measurement stations in Arctic regions since mid-20th century to early 2000, as opposed to the global trend of decline in near surface rates (McVicar et al., 2012), which may have long-term impacts on atmospheric evaporative demand. These changes have important implications for land-atmosphere processes, including multiple feedbacks on climate, such as the feedback between warming and the reduction in ice extent that has altered vegetation distributions, and

* Corresponding author at: 1 Cyclotron Rd, Berkeley, CA 94720, USA.
E-mail addresses: rynaama@gmail.com (N. Raz-Yaseef), mstorn@lbl.gov (M.S. Torn).

http://dx.doi.org/10.1016/j.jhydrol.2017.08.036
0022-1694/Published by Elsevier B.V.

increased emissions of CO_2 and methane from thawing permafrost (Chapin et al., 2000, Hinzman et al., 2013, Schuur et al., 2015). Data-rich, landscape-level studies have the potential to improve our understanding of how changes in ecosystem fluxes can mitigate or enhance further warming.

This study focused on understanding how variations in geomorphology and vegetation control evapotranspiration (ET) on the Alaskan Arctic tundra coastal plain near Barrow, AK, USA. ET is the total vapor flux from land to atmosphere, which is the combined flux of direct evaporation, plant transpiration, intercepted precipitation, and sublimation. The evaporation component of ET includes the flux from bare ground and open water, as well as from nonvascular mosses and lichens, which do not transpire. The importance of ET is multitudinal: it is a key component in the hydrological cycle and the land energy balance, it affects plant distribution and productivity, and as a greenhouse gas, it generates feedbacks with climate.

Microtopographic differences (at the meter scale) are correlated with environmental factors such as soil moisture, geochemistry, soil nutrients, and soil temperature (Kane et al., 1990; Heikoop et al., 2015; Lara et al., 2015; Newman et al., 2015; Throckmorton et al., 2016; Wainwright et al., 2015). Polygonal geomorphology is caused by freeze-thaw cycles and the expansion and contraction of ice wedges extending from the permafrost to the near surface. One common polygon pattern is low topographical centers surrounded by elevated edges. With prolonged thaw, the ice wedges supporting the polygon's edges degrade, resulting in high topographical centers, and thus a transition between low-centered and high-centered polygons. Troughs form between polygons, creating low-elevation borders around polygons. While troughs and low polygon centers are wet or inundated, high polygon centers and the elevated edges of all polygons are drier. In turn, these microtopographic differences control plant distributions: drier and warmer areas such as polygon edges and high polygon centers tend to have more lichens, grasses, and bare ground. In low polygon centers and troughs, which are wetter or inundated, mosses and sedges are more frequent. Plant distribution affects surface albedo and energy balance, biogeochemistry, and microbial activity (Andresen et al., 2016; Chapin et al., 1996; Stoy et al., 2012; Villarreal et al., 2012; Heikoop et al., 2015; Newman et al., 2015), but less is known about how microtopography-controlled plant distributions affect ET.

ET is the major pathway for water loss in the Barrow region, sometimes exceeding summer precipitation (Mather and Thornthwaite, 1958; Clebsch and Shanks, 1968, Kane et al., 1990; Mendez et al., 1998). Previous studies measured daily ET values in pond-free areas in Barrow in the range of 0.8–1.8 mm d^{-1} (Mather and Thornthwaite, 1958; Kane et al., 1990). The spatial heterogeneity of ET is still highly uncertain and its representation in models is poor due to sparse measurement and large natural variability (Zhang et al., 2009, Liljedahl et al., 2011).

Lichens and mosses are abundant in Arctic tundra (Oechel and Van Cleve, 1986), and have a large impact on ecosystem traits and processes such as surface energy partitioning, peat accumulation, fires, and gas exchange (Addison, 1975; Beringer et al., 2001; Douma et al., 2007; Turetsky et al., 2012). Mosses are major contributors to ET in tundra environments not only because of their high abundance, but also because of their high porosity and high water-holding capacity, lack of control over water loss to the atmosphere due to the lack of stomata and roots, and ability to move water from the substrate through capillary action (Beringer et al., 2001; Heijmans et al., 2004; Engstrom et al., 2006). In addition to evaporation from non-vascular plants, open water evaporation can also be substantial because of the widespread lakes, ponds, and other inundated areas in the Arctic coastal plain (Andresen and Lougheed, 2015; Koch et al., 2014; Throckmorton et al., 2016).

Our objectives in this study were to: (1) Evaluate the influence of plant type on the spatial variability of ET; (2) Evaluate the influence of polygonal microtopography on the spatial variability of ET; and (3) Define the inter-correlation between plant type and microtopography describing the spatial variability of ET in polygonal tundra.

To address the research objectives, we measured ET of the main vegetation types (mosses, grasses and forbs, sedges and lichens), non-vegetated surfaces (open water and bare ground), and geomorphologic units (low polygonal centers, high polygonal centers, polygonal edges, and troughs) of the tundra with a portable chamber. ET was also measured with two continuous systems: a flux tower and an automatic soil chamber, from thaw to snow-in. Measurements were organized to assess multi-scale controls on ET. We also compared carbon fluxes (CO_2 and CH_4) to ET, to characterize the seasonal pattern of each. Plot-scale portable measurements were used to assess the contributions of different landscape components, and continuous measurements were used to characterize diurnal and seasonal patterns.

2. Materials and methods

2.1. Research site

The Barrow Environmental Observatory (BEO, 71.29° N, 156.61° W) is located near the coastal village of Barrow, Alaska, on the north slope of the Brooks Range (Fig. 1).

Elevation differences between the top of polygonal edges and the bottom of troughs are roughly 1 m (Gamon et al., 2012; Hubbard et al., 2013). The maximum active layer depth is approximately 50 cm, underlain by thick, continuous permafrost (Gangodagamage et al., 2014). Between 1949 and 2014, mean annual air temperature was −12 ± 4 °C and mean annual precipitation was 180 ± 51 mm yr^{-1} (Barrow Willey Post-Will Rogers Airport Meteorological Station, Alaska, USA), with approximately half of the precipitation falling as rain during the short summers. Soils are generally classified as Gelisols, and are characterized by an organic-rich surface layer underlain by a silt-loam mineral layer. The vegetation is dominated by graminoids (*Carex aquatilis*, *Eriophorum* spp. *Luzula* spp.) and non-vascular constituents such as mosses (e.g., *Sphagnum* spp., *Drepanocladus* spp.) and lichens, with some forbs and occasional dwarf shrubs (Sturtevant and Oechel, 2013; Wullschleger et al., 2014).

Portable chamber ET measurements were preformed in the BEO in an intensive research zone comprising four areas located near the eddy flux tower (A to D; Fig. 1(b)). Areas A and D are dominated by low-centered polygons (although A shows more signs of degradation than D), and areas B and C contain a high proportion of high-centered and flat-centered polygons (i.e., topographically elevated centers). The four areas thus represent a range of microtopographic conditions, making the BEO intensive research area an ideal site for examining ET variations in a polygonal tundra landscape.

2.2. Eddy covariance tower and meteorological measurements

An eddy covariance tower was installed at the BEO in September 2012 (AmeriFlux ID US-NGB). The main instruments in this system are a Gill-Solent sonic anemometer (Gill R3-50, Gill Instruments, UK), a LI-COR CO_2/H_2O open-path infrared gas analyzer (LI-7500A, LI-COR Biosciences, NE, USA), and a LI-COR open-path CH_4 infrared gas analyzer (LI-7700, LI-COR Biosciences, NE, USA). Instruments were located 4 m above the ground. Turbulent vertical fluxes of CO_2, H_2O, and CH_4 were calculated half-hourly using algorithms for spike removal, coordinate rotation to zero mean vertical and cross wind speed, and block averaging of scalar quantities

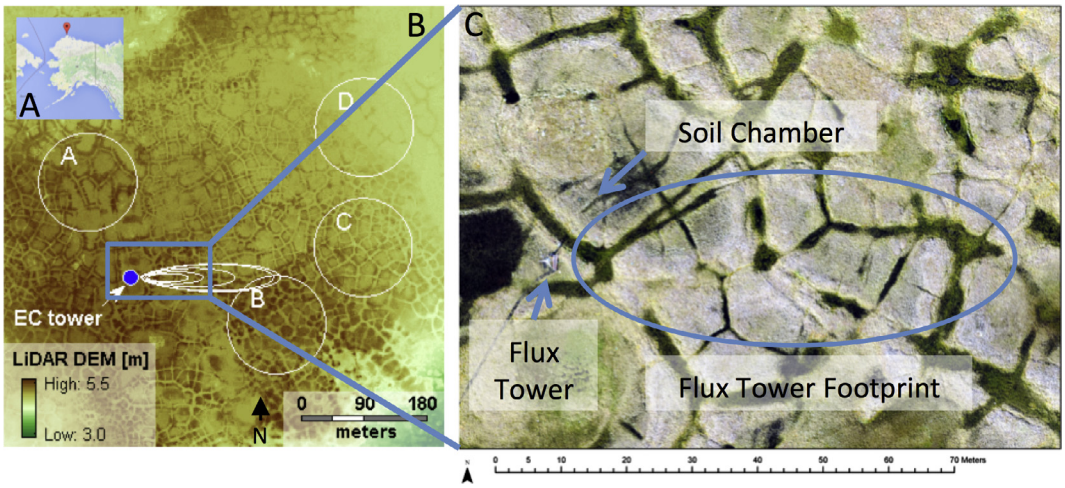

Fig. 1. (A) The field site is located near Barrow, on the coast of the Arctic Ocean. (B) Polygon microtopography at the research site captured by LiDAR. Location of the flux tower and footprint (white ellipse) are shown. Measurements with the portable chamber were conducted in areas A to D. (C) The location of the automatic soil chamber and eddy-covariance tower. The main flux tower's footprint (>50% of time) is shown (blue ellipsoid).

(Billesbach et al., 2004). Density corrections were applied to the covariances of vertical wind, using CO_2 and H_2O densities obtained with the open-path infrared gas analyzer (IRGA; Billesbach et al., 2004). Random uncertainties in measured fluxes, obtained from averaging turbulence measurements, were estimated to be approximately 10% (Billesbach, 2011). Footprint analysis was conducted according to the Detto et al. (2006) 2D extension to the Hsieh et al. (2000) model. Gaps in the CO_2 and CH_4 record were filled using a method based on Marginal Distribution Sampling (MDS) (Reichstein et al., 2005). Because of harsh winter conditions, the BEO eddy covariance system was not operated between November and May. A system failure resulted in no measurements from mid-May to mid-June in 2014. During the non-operational months, the trace gas instruments were returned to the laboratory (Lincoln, NE, USA) for cleaning, maintenance, and calibrations. For further information about the flux tower and data analysis refer to Billesbach et al. (2004), Billesbach, (2011) and Raz-Yaseef et al. (2016).

Radiation sensors were installed on an extending arm on the flux tower at 3.20 m above ground. The measurements included short- and long-wave upwelling and downwelling radiation (CNR4, Kipp & Zonen, Delft, The Netherlands), upwelling and downwelling photosynthetic active radiation (PAR) (2 x LI-190 Quantum Sensors, LI-COR Biosciences, NE, USA), and surface skin temperature (down-looking SI-111 infrared radiometer, Apogee Instruments, UT, USA). Albedo was calculated from radiation measurements for each half-hour. Sensors calibration and maintenance are described by Billesbach et al. (2004). Wind speed and direction were measured by the sonic anemometer. Air temperature and relative humidity (50-Y Humitter, Vaisala, Finland, housed in REBS 6-plate, non-aspirated radiation shields), and air pressure (PT-101 B, Vaisala, Finland) were measured at 3 m above ground.

Subsurface temperature measurements were made along a 17.4 m transect from a polygon center to a trough in each of the four areas; data from area A are reported here (Fig. 1(B)). Five vertical arrays were installed along the transect, each measuring at 16 depth points, from the surface to 1.5 m depth (http://dx.doi.org/10.5440/1126515). Measurements were made with thermistor probes every 5 minutes. The probes were connected to a CR1000 data logger (Campbell Scientific, Inc., UT, USA), and hourly averages were stored on the logger. Prior to installation the thermistors were calibrated in an ice bath to achieve an accuracy of approximately ±0.02 °C at 0 °C. Soil temperatures used in this study are an average of all five vertical arrays for each defined soil layer.

2.3. Surface ET

2.3.1. Stationary automated chamber

We used an adapted LI-8100A-104C automated soil CO_2 flux system (LI-COR Biosciences, NE, USA) with a clear chamber, that was previously tested at the field site for quantifying ET (Cohen et al., 2015). The flux system has an automatic arm that moves the chamber over a soil collar and lowers it to create a seal with the collar. Once the measurement is done, the arm lifts the chamber away from the soil collar, to minimize disturbance. Water fluxes were estimated from vapor concentration measurements using LI-8100A File Viewer 3·2c software with a linear fit over the first 10 seconds of measurement using Eq. (1) from Raz-Yaseef et al. (2010) and LI-COR manuals:

$$E = C\frac{dH}{dt}\frac{V}{A}\frac{P}{T_a R} \quad (1)$$

where E is the water vapor flux (mmol H_20 m^{-2} s^{-1}), C is the correction factor determined for the instrument through calibration, dH/dt is the measured rate of change in water vapor concentration with time inside the chamber (mmol H_20 mol^{-1} air s^{-1}), V is the chamber volume (m^3), A is the surface area in the collar (m^2), P is the chamber pressure (Pa), T_a is the chamber air temperature (K), and R is the gas constant (J mol^{-1} K^{-1}).

The Li-8100A was installed near the edge of a high-centered polygon, approximately 17 m north of the tower (Fig. 1(C)). Vegetation inside the collar was a mixture of lichens, grasses, and mosses, in the order of decreasing area cover. The analyzer was deployed from 18 June until 10 September 2013, and a measurement was taken every 15–30 min.

2.3.2. Portable chamber

To measure spatial variability and a wide range of surface conditions, we deployed a portable system using a chamber connected to a LI-6400 IRGA (LI-COR Biosciences, NE, USA). A cylindrical 10-cm tall extension constructed from clear plexiglass was attached to the bottom of the LI-6400 soil respiration chamber, after Raz-Yaseef et al. (2010). By increasing the chamber volume, the extension compensated for the larger flux of water in comparison to CO_2 for which the respiration chamber was designed, extending the period of time in which the water flux is nearly linear. We used clear plexiglass so that light could reach the surface vegetation and soil. This modified chamber system was utilized with the LI-6400

console in the same way that the soil respiration system is used for soil CO_2 flux measurements. ET was calculated based on Eq. (1). Twenty-four hours prior to measurements, 7 cm-tall PVC collars were inserted into the ground to a depth of 4 cm at each measurement location. During measurement, the chamber with plexiglass extension was placed on the PVC collar for 30–60 s. As with the automated system, ET was calculated based on changes in water vapor during a short period immediately after chamber placement on the collar, when $dH/\delta t$ is still linear and not affected by the accumulation of vapor in the chamber, typically 10–15 s.

2.4. Field campaign

A field campaign was carried out to sample ET from the range of plant types at the BEO. To choose locations for measurements with the portable chamber, we conducted a plant survey within areas A–D (Fig. 1(B)). For each plant type, we identified between 3 and 7 locations in which the given plant type was dominant in an area larger than the chamber base, thus allowing each measurement to characterize a single type with minimal contribution for other types. Measurements were made for the following categories: (1) Sedges (*Eriophorum russeolum*, *Carex aquatilis*, *Eriophorum* spp., *Dupontia fisheri*, *Arctophila fulva*, *Eriophorum angustifolium*); (2) Grasses (*Luzula arctica*, *Poa arctica*, *Arctagrostis latifolia*); (3) Forbs (*Saxifraga foliolosa*, *Petasites frigidus*); (4) Shrubs (*Vaccinium vitis-idaea*, *Salix pulchra*); (5) Mosses (dominated by *Polytrichum* spp.); (6) Lichens (*Alectoria* spp., *Cladonia* spp., *Dactylina arctica*); (7) Open water; and (8) Bare ground.

Field measurements using the portable chamber were made during one-week campaigns in late July 2013 and early July 2014. Measurements were made from ~9:00 am to 5:00 pm AKST in non-raining conditions. In 2013, 23 soil collar locations were measured and in 2014, 43 locations were measured. During each measuring day, one or two complete repetitions of all collars were conducted, depending on weather conditions. Soil temperature (AquaTuff thermocouple temperature probe, Cooper Atkins, CT, USA) and soil moisture (MiniTrase Time Domain Reflectometry, Soilmoisture Equipment Corp., CA, USA) were measured adjacent to each soil collar.

3. Results

3.1. Meteorological conditions

In high-latitude regions, irradiance is low even in summer, and at Barrow, 24-h average incoming short-wave radiation in June-July-August was between 100 and 380 W m^{-2} (Fig. 2(A)), depending on cloud cover and time of day. In 2013 and 2014, thaw occurred between 29 May and 10 June, when air temperatures rose above freezing (Fig. 2(B)). Snowmelt took place in early June, when

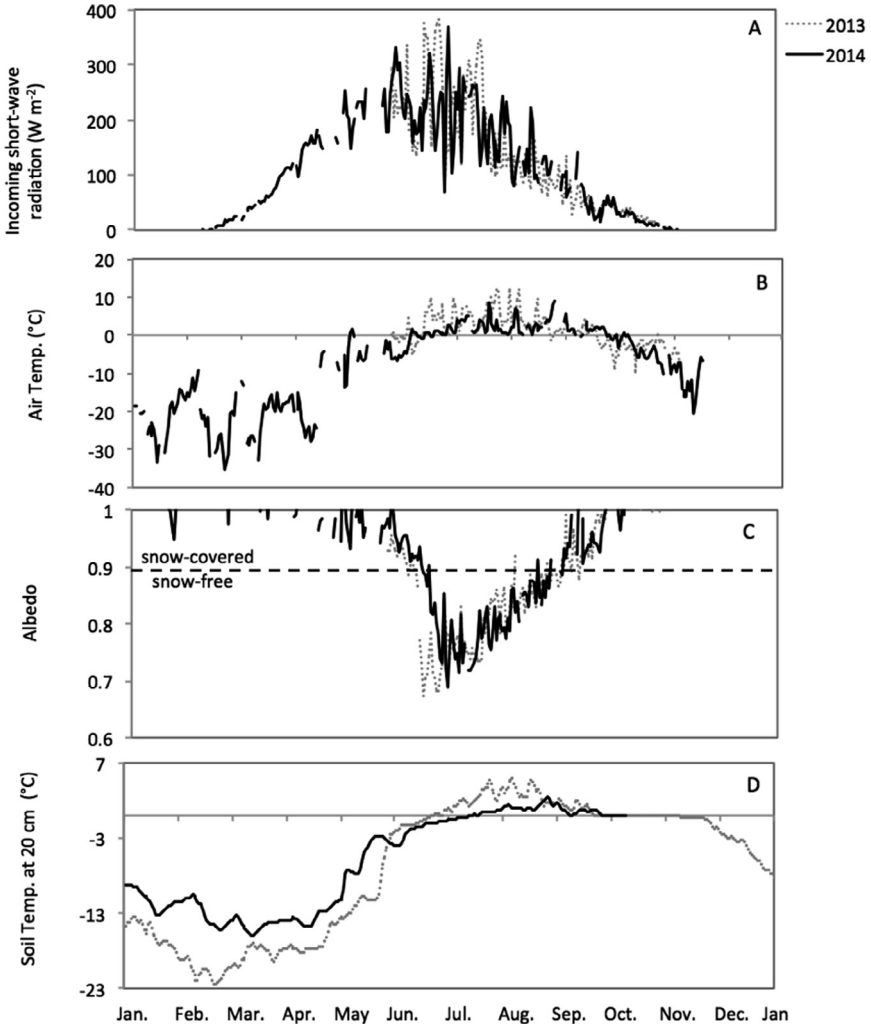

Fig. 2. Daily average meteorological conditions measured at the BEO in 2013 and 2014 for (A) incoming short-wave radiation, (B) air temperature, (C) albedo, and (D) soil temperature at a depth of 20 cm. Based on ground measurements at the field site, we used an albedo threshold of 0.89 to distinct between snow-covered and snow-free ground. The summer of 2013 was longer and warmer.

albedo dropped below 0.9 (Fig. 2(C)). By early July, the active layer thickness was about 20 cm (Fig. 2(D)).

Active layer thickness is spatially variable over the site, and in 2013 and 2014, maximum active layer thickness in most places was less than 40 cm, with some locations extending below 50 cm (using poking stick, data not shown). By early to mid-September, maximum incoming short-wave radiation dropped below 100 W m^{-2} and air temperatures dropped below 0 °C. Snow covered the ground, and albedo was close to 1. By early October, freezing of the active layer had begun, and winter conditions persisted until May.

We observed differences in meteorological conditions between the two measured years. In 2014, the snow-free season was 71 days compared to 89 days in 2013, and mean June-July-August air temperature was 1.8 °C, compared to 3.9 °C in 2013. The shorter and colder summer in 2014 relative to 2013 affected ecosystem fluxes, as discussed below. Although summer 2014 was on average cooler than in 2013, conditions during the weeks of the two portable chamber campaigns were the opposite, with more frequent overcast and cooler temperatures in the campaign days of 2013.

3.2. Ecosystem fluxes

Early in the season, ET was not significantly different than zero (daily average <0.02 mm h^{-1}), but ET began to increase soon after thaw. Daily average ET rates displayed a steep and rapid rise in spring, peaking in early July (fluxes up to 0.14 mm h^{-1}), and a longer and more gradual decrease in fall (Fig. 3(A)).

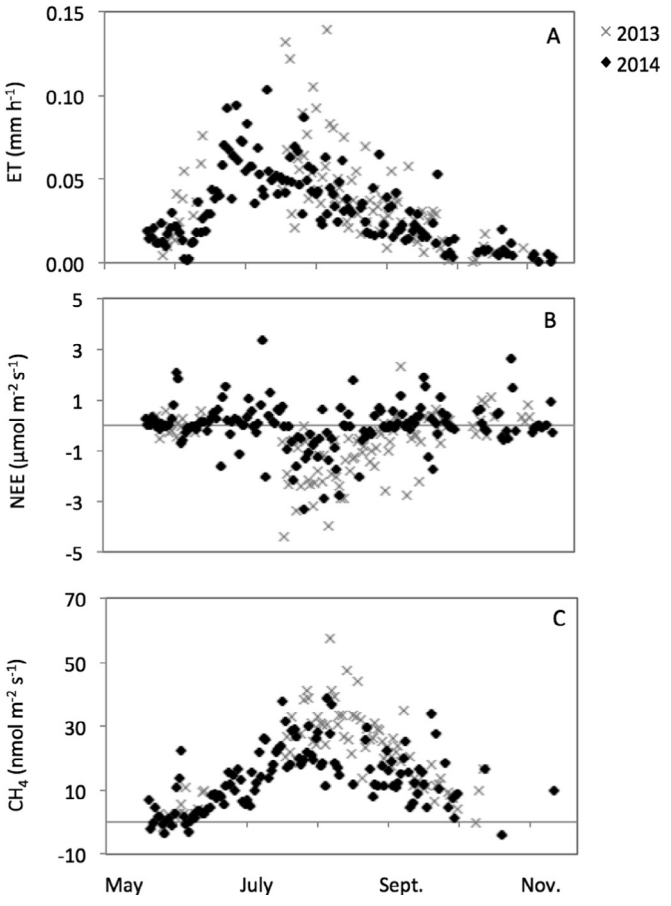

Fig. 3. Daily averages of ecosystem fluxes measured by the flux tower in 2013 and 2014 for (A) ET, (B) NEE (negative fluxes denote net CO_2 uptake from atmosphere), and (C) CH_4. After snowmelt at end of May, ET increases rapidly and peaked in early July; CO_2 uptake and CH_4 emissions increase more gradually and peaked in late July to early August. By the end of September, fluxes decreased to near-zero. The measurement gap in 2013 was due to power outage.

The timing of peak ET and the seasonal trend in ET differed from that of the carbon fluxes (CO_2 and CH_4) (Fig. 3(B) and Fig. 3(C)). Carbon fluxes peaked later in the season – late July to early August, and in comparison to the steep climb of ET, the carbon fluxes increased and decreased gradually and were more symmetrical seasonally. The length of the non-zero ET-flux season, the timing of peak fluxes, and the seasonal range in daily fluxes varied between the two years: peak daily ET during the warmer summer of 2013 was up to 35% higher than peak daily ET during the cooler summer of 2014. In June-July-August, ET had a clear diurnal cycle (Fig. 4), and the variation in half-hour values in ET were closely correlated with downwelling shortwave radiation ($R^2 = 0.74$ between ET and shortwave radiation for all half-hour periods from June to August 2014; results not shown).

3.3. Spatial variability of ET

Based on the portable chamber measurements, there was high variability in ET across the field site. Comparing surface-cover types, fluxes were highest over mosses and open water, lower from grasses and sedges (~65% of those from mosses and open water), and lowest over bare ground and lichens (~50% of those from mosses and open water; Fig. 5 and Table 1).

Chamber fluxes were higher in 2014 than in 2013, but the relationships between ET and plant types remained the same. Grouping portable chamber measurements by microtopography (Fig. 6) showed that ET was highest over troughs, lower from low-centered polygons (area A in Fig. 1(B); ET ~ 90% of trough), and lowest from high-centered polygons (area B in Fig. 1(B); ET ~ 50% of trough).

Our two continuous systems sampled different parts of the landscape; the automated chamber measured a relatively dry area while the tower footprint always included some wetter areas. Flux towers have a large and time-varying fetch. For the dominant footprint at our site—accounting for more than 55% of the time—more than 50% of the flux measured by the flux tower originated from a 70 m long ellipsoid-shaped area east of the tower, marked in Fig. (1(C)). Most of the area in this footprint was in centers and troughs of low-centered polygons, which have open water and high areal abundance of mosses. The rest of the footprint area to the east (i.e., the 90% influence area) also included inundated and moist areas. The rest of the time, the footprint was fairly evenly distributed in the other directions, and always contained some wet or inundated areas. The automated chamber was located on a dry spot of a polygonal edge near the flux tower, with a high abundance of lichens and bare ground (Fig. 1(C)). The two continuous systems showed similar seasonal trends but with different magnitude: ET measured by the automated chamber was only 44% of flux tower ET (n = 56 days, STD = ±41%; Fig. 4 shows both automated chamber ET and flux tower ET for a part of this period, during the summer campaigns). The large variation between flux tower and portable chamber measurements is related to changes in the tower's footprint size and location. Portable chamber measurements over lichens and grasses were similar to those measured by the automated chamber, and portable chamber measurements over open water and mosses were similar to those measured by the flux tower. Accordingly, measurements conducted with the automated chamber aligned with the lower end of the portable chamber measurements, representing dry areas (polygon edge, cover of mainly lichens and forbs), and the eddy flux measurements matched the high end of the portable chamber measurements, with flux sourcing over wetter areas (Fig. 4).

To investigate how our measurements of ET translate to the landscape scale, we combined our point-scale portable chamber

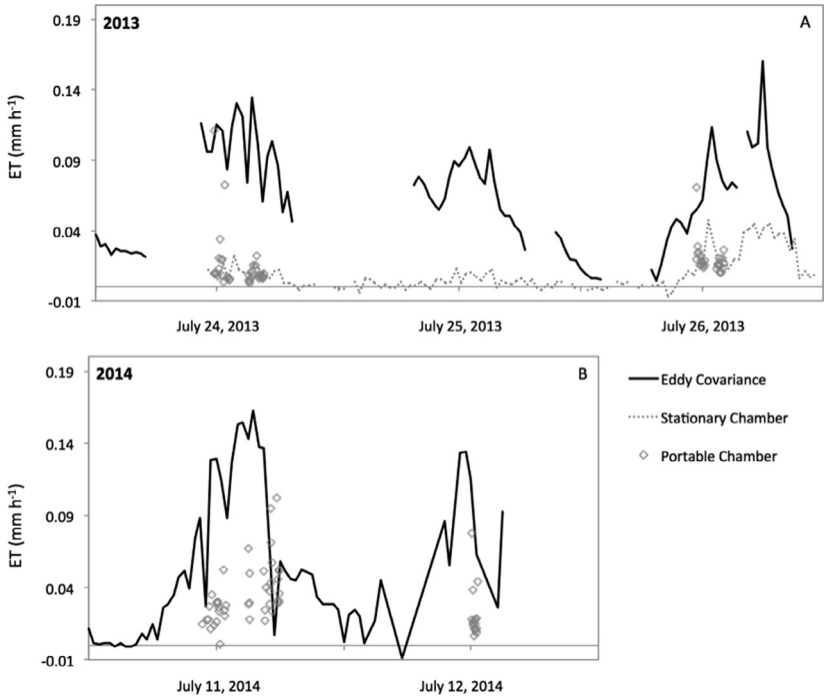

Fig. 4. Half-hourly ET during selected days of the field campaign in (A) 2013 and (B) 2014. Measurements conducted with the portable chamber over different vegetation types and surface cover types showed a large range in ET. The automated chamber (used only in 2013) was located on a polygonal edge (dry, mostly lichens), and matched the lower range of portable chamber fluxes. The eddy flux tower, whose footprint included significant areas of wet vegetation (mosses and sedges) and inundation, matched the higher end of portable chamber fluxes. Gaps in eddy flux measurements occurred when the eddy flux data did not meet QA/QC requirements, mainly at nighttime.

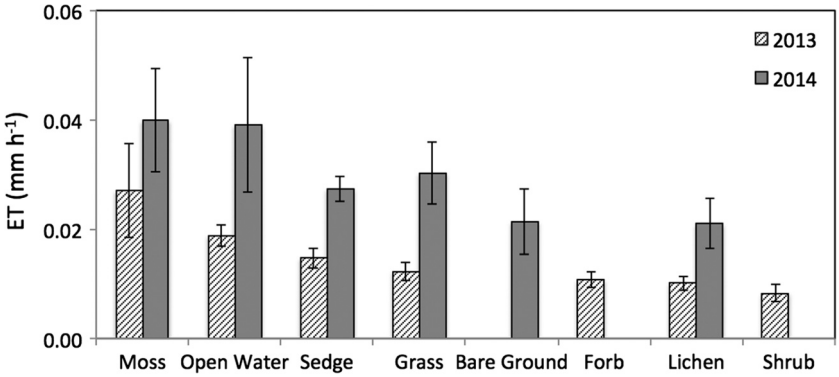

Fig. 5. ET measured with the portable chamber in 2013 and 2014. Values are averages for each plant type and for open water; bars denote standard deviation. More information is available in Table 1. Highest fluxes were measured over moss-covered areas and open water; lowest fluxes over bare ground and lichens.

Table 1
ET rates measured with the portable chamber in each year and for each plant type. Standard deviation (STD) and sample size (*n*) are also shown.

Year	ET (mm h^{-1})	Moss	Open Water	Grass	Sedge	Bare Soil	Forb	Lichen	Shrub
2013	Average	0.027	0.019	0.012	0.015		0.011	0.010	0.008
	STD	0.009	0.002	0.002	0.002		0.001	0.001	0.002
	n	7	6	7	14		9	8	
2014	Average	0.040	0.039	0.030	0.027	0.021		0.021	
	STD	0.01	0.01	0.01	0.00	0.01		0.00	
	n	11	8	5	24	3		6	

measurements with remote sensing surveys of plant distribution of the field site (Langford et al., 2016). According to this survey, wet vegetation (mosses and sedges) and open water accounted for more than 70% of ground cover in the main flux tower footprint, east of the tower. Wet vegetation and open water accounted for only 50% in areas A–D (Table 2).

Combining areal coverage with cover-specific ET (Table 1), we estimated the relative contribution of each ground cover to ET (Fig. 7).

ET from mosses, sedges and open water alone contributed nearly 80% of ET in the flux tower footprint area (Fig. 1(B)), and about 58% of total ET in areas A–D (Fig. 1(A)), which had less

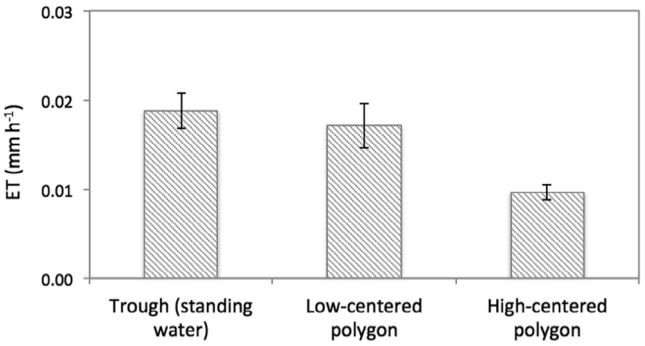

Fig. 6. ET measured with the portable chamber in 2013 (average flux and standard deviation) over troughs ($n = 6$), low-centered polygons ($n = 28$), and high-centered polygons ($n = 26$). The low polygonal centers are inundated, have more mosses, and produce higher ET than high polygonal centers.

open water. With high ET and high percentage of ground cover, the contribution of these three landscape components to ET was substantial. Bare ground was the most common cover type in the centers of areas A - D (30%, Table 2), but its contribution to total ET was lower than that of mosses, because of the low flux per unit area.

4. Discussion

Although topographical variations in coastal Arctic polygonal tundra are merely on the order of 1 m (Hubbard et al., 2013), elevated geomorphological structures (polygon edges and high polygonal centers) and low structures (troughs and low polygonal centers) create different micro-environments (Fig. 8).

Low topographical structures are often inundated or saturated due to poor drainage, leading to higher abundance of wet tundra vegetation – mosses and sedges (Langford et al., 2016). The combination of moist soils that produce high evaporation rates and vegetation types that produce high transpiration both contribute to the overall high ET from troughs and low polygonal centers. In elevated locations, lower soil moisture creates an advantage for lichens and forbs, and the combination of dry soils that produce low evaporation rates and vegetation types that produce low transpiration both contribute to the overall low ET from edges and high polygonal centers.

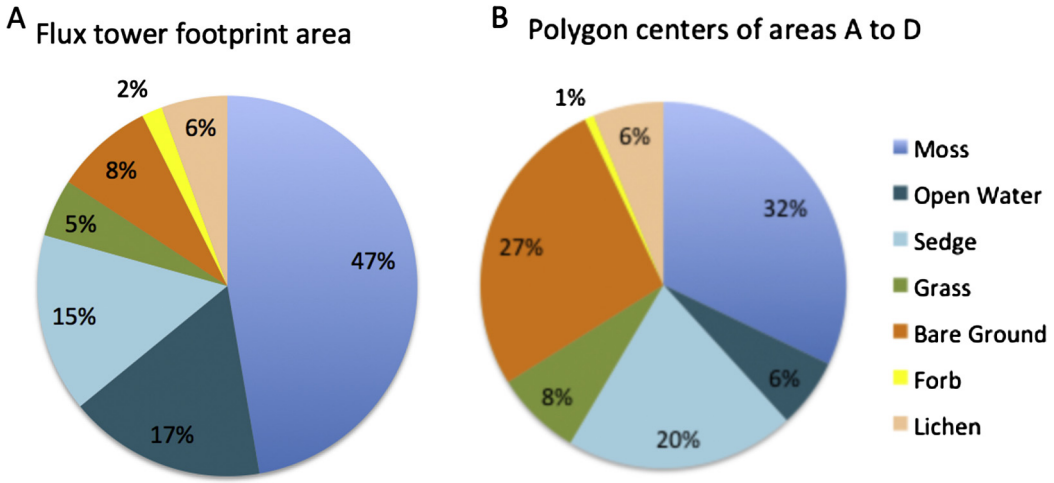

Fig. 7. The relative contribution of each plant and surface-cover type to total ET for (A) the flux tower footprint area (Fig. 1(C)), and (B) an average for polygon centers of areas A–D (Fig. 1(B)). Results are based on ET presented in Table 1 and plant distribution presented in Table 2.

	Microtopographic High areas	**Microtopographic Low areas**
Geomorphological unit	Polygonal edges High polygonal centers	Troughs Low polygonal centers
	↓	↓
Soil moisture	Low	High / inundated
Soil temperature	High	Low
	↓	↓
Vegetation type	Lichens, grasses	Moss, sedges
	↓	↓
ET	Low	High

Fig. 8. Schematic diagram of the effect of microtopography on the spatial patters of ET.

Table 2
Distribution of vegetation ground coverage (%) for the tower footprint area (Fig. 1(C)) and for polygon centers of areas A to D (Fig. 1(B)), calculated after Langford et al. (2016).

Ground cover (%)	Moss	Open Water	Sedge	Grass	Bare Ground	Forb	Lichen	Total
Tower footprint	37	15	19	6	10	4	9	100
Areas A-D centers	23	5	23	8	30	2	9	100

In a synthesis of environmental and climatic observations over the past few decades Hinzman et al. (2013) found that there is high statistical confidence that overall ET has an increasing trend in the Arctic, but they found low agreement in the size of this change among different locations due to high spatial and temporal variability. Indeed, the large heterogeneity of ET observed in our research is derived from the spatial distribution of microtopographic and vegetation types, which are not uniform across the Arctic landscape.

Temporal patterns in ET reflected patterns in downwelling radiation, snowmelt, vegetation processes, and other conditions. Even under 24 hours of daylight, there was sufficient variation in shortwave radiation to give ET a strong diurnal pattern (Stuart et al., 1982). The seasonal trend in ET differed from that of the carbon fluxes (CO_2 and CH_4) (Fig. 3(B) and (C)), revealing a decoupling between carbon and water fluxes. We attribute the rapid rise in ET, and its peak earlier in the year than that of peak carbon fluxes, to a high contribution of evaporation (E) to ET. Evaporation from inundated areas and mosses, which is controlled mainly by radiation, can start early in the season as soon as temperatures rise above zero and liquid water is available at the surface. Transpiration and CO_2 uptake lag evaporation, being dependent on the accumulation of green leaf area (Nosko and Courtin, 1995). Moreover, Young-Robertson et al. (submitted for publication), using stable isotopes at this field site, showed that evaporation dominates ET in July (in other words there is high evaporation even when leaf area is high), consistent with attributing the early season rise in ET to high E rates soon after thaw.

Not only is there large spatial and temporal variability in the geomorphic and climatic drivers of ET, but the way in which these drivers will change over time is itself variable, making it difficult to predict future ET. In northern latitudes, warming trends and changes in precipitation are expected to affect the polygon structure and active layer thickness of tundra ecosystems (Hinzman et al., 2005; Liljedahl et al., 2016; Spielhagen et al., 2011). As a result, changes in vegetation distributions across the Arctic are expected to increase in rate and extent (Tape et al., 2006, Goetz et al., 2011, Pearson et al., 2013). All of these trends will influence the distribution of ET over the Arctic. However, it is challenging to relate the microtopographic/vegetation distribution control on ET that this study demonstrates to specific future landscape trends. As an example of the complexity of such predictions, consider the following case. In the Barrow region, ice wedge degradation over recent decades has increased the areal abundance of troughs, and decreased the abundance of low-centered polygons (Liljedahl et al., 2016). Our study suggests that increases in troughs would tend to increase ET over this region, but development of high-centered polygons would create new areas with relatively low ET. Thus, it is difficult to project the net effect without details on the spatial extent of changes related to degraded permafrost. While changes in ET can generate climate change feedbacks (Swann et al., 2010), the same landscape changes that affect ET, like shifts from low- to high-centered polygons, may result in negative feedbacks to warming (Lara et al., 2015) via decreases in CO_2 and CH_4 fluxes, mediated by changes in soil moisture content and vegetation type.

What seems most critical for understanding future shifts in ET is to couple the effects of longer growing seasons with better spatial assessments of polygon types, lakes, and ponded areas, and how these features and their associated vegetation types are changing over time. Some regions and sites of degraded permafrost landscapes will become drier while other areas will become much wetter (Hinzman et al., 2013). To scale-up ET observations to a larger scale (e.g., an Earth Systems Model grid), our study shows the necessity of mapping microtopography and it's related plant distributions. Fortunately, advances in high-resolution spatial analysis and remote sensing can aid in monitoring future landscape changes (e.g., Gangodagamage et al. 2014, Lara et al., 2015, Andresen and Lougheed, 2015, Langford et al., 2016), which should make it more feasible to quantify how the pattern of ET is changing.

5. Conclusion

Rates of ET varied by two-fold across the arctic polygonal tundra near Barrow, Alaska, and variability in microtopography was the main driver for this spatial variability. Each microtopographic location was associated with specific plant types, and the combination of geomorphic unit and plant type created large spatial variability in ET. Both plant distribution and microtopography are important to incorporate in estimates or predictions of ET in the Arctic.

Acknowledgements

The Next-Generation Ecosystem Experiments (NGEE Arctic) project is supported by the Office of Biological and Environmental Research in the DOE Office of Science. We thank Lily Cohen and Bryan Curtis for field and laboratory support. We thank Zachary Langford and Jitendra Kumar for providing information on plant cover distribution. We thank two anonymous reviewers, the Associate Editor, and Editor, whose thorough editing and thoughtful suggestions helped improve this manuscript.

References

Addison, P.A., 1975. Studies on evapotranspiration and energy budgets on Truelove Lowland. In: Bliss, L.C. (Ed.), Truelove Lowland, Devon Island, Canada: A High Arctic Ecosystem. University of Alberta Press, Edmonton, Alberta, pp. 281–301.

Andresen, C.G., Lougheed, V.L., 2015. Disappearing Arctic tundra ponds: fine-scale analysis of surface hydrology in drained thaw lake basins over a 65 year period (1948–2013). J. Geophys. Res. Biogeosci. 120. http://dx.doi.org/10.1002/2014JG002778.

Andresen, C.G., Lara, M.J., Tweedie, C.E., Lougheed, V.L., 2016. Rising plant-mediated methane emissions from arctic wetlands. Global Change Bio. http://dx.doi.org/10.1111/gcb.13469.

Beringer, J., Lynch, A.H., Chapin, F.S., Mack, M., Bonan, G.B., 2001. The representation of arctic soils in the land surface model: the importance of mosses. J. Clim. http://dx.doi.org/10.1175/1520-0442(2001) 014<3324:TROASI>2.0.CO;2.

Billesbach, D.P., Fischer, M.L., Torn, M.S., Berry, J.A., 2004. A portable Eddy covariance system for the measurement of ecosystem-atmosphere exchange of CO_2, water vapor, and energy. J. Atmos. Ocean. Technol. 21, 639–650. http://dx.doi.org/10.1175/1520-0426(2004) 021<0639:APECSF>2.0.CO;2.

Billesbach, D.P., 2011. Estimating uncertainties in individual eddy covariance flux measurements: a comparison of methods and a proposed new method. Agric. For. Meteorol. 151, 394–405. http://dx.doi.org/10.1016/j.agrformet.2010.12.001.

Chapin, F.S., Bret-Harte, M.S., Hobbie, S.E., Zhong, H., 1996. Plant functional types as predictors of transient responses of arctic vegetation to global change. J. Vegetation Sci. 7 (3), 347–358.

Chapin, F.S., Mcguire, A.D., Randerson, J., Pielke, R., Baldocchi, D., Hobbie, S.E., Roulet, N., Eugster, W., Kasischke, E., Rastetter, E.B., Zimov, S.A., Running, S.W., 2000. Arctic and boreal ecosystems of western North America as components of

the climate system. Glob. Change Biol. 6, 211–223. http://dx.doi.org/10.1046/j.1365-2486.2000.06022.x.
Clebsch, E.E.C., Shanks, R.E., 1968. Summer climatic gradients and vegetation near barrow, Alaska. Arctic 21 (3), 161–171.
Cohen, L.R., Raz-Yaseef, N., Curtis, J.B., Young, J.M., Rahn, T.A., Wilson, C.J., Wullschleger, S.D., Newman, B.D., 2015. Measuring diurnal cycles of evapotranspiration in the Arctic with an automated chamber system. Ecohydrology 8, 652–659. http://dx.doi.org/10.1002/eco.1532.
Detto, M., Montaldo, N., Albertson, J.D., Mancini, M., Katul, G., 2006. Soil moisture and vegetation controls on evapotranspiration in a heterogeneous Mediterranean ecosystem on Sardinia, Italy. Water Resour. Res. 42 (8).
Douma, J.C., Van Wijk, M.T., Lang, S.I., Shaver, G.R., 2007. The contribution of mosses to the carbon and water exchange of Arctic ecosystems: quantification and relationships with system properties. Plant. Cell Environ. 30, 1205–1215. http://dx.doi.org/10.1111/j.1365-3040.2007.01697.x.
Engstrom, R., Hope, A., Kwon, H., Harazono, Y., Mano, M., Oechel, W., 2006. Modeling evapotranspiration in Arctic coastal plain ecosystems using a modified BIOME-BGC model. J. Geophys. Res. 111, G02021. http://dx.doi.org/10.1029/2005JG000102.
Gamon, J.A., Kershaw, G.P., Williamson, S., Hik, D.S., 2012. Microtopographic patterns in an arctic baydjarakh field: do fine-grain patterns enforce landscape stability? Environ. Res. Lett. 7, 015502. http://dx.doi.org/10.1088/1748-9326/7/1/015502.
Gangodagamage, C., Rowland, J.C., Hubbard, S.S., Brumby, S.P., Liljedahl, A.K., Wainwright, H., Wilson, C.J., Altmann, G.L., Dafflon, B., Peterson, J., Ulrich, C., Tweedie, C.E., Wullschleger, S.D., 2014. Extrapolating active layer thickness measurements across Arctic polygonal terrain using LiDAR and NDVI data sets. Water Resour. Res. 50, 6339–6357. http://dx.doi.org/10.1002/2013WR014283.
Goetz, S.J. et al. in Eurasian Arctic Land Cover and Land Use in a Changing Climate (eds Gutman, G. & Reissell, A.) 9–36 (Springer, 2011).
Heijmans, M.M.P.D., Arp, W.J., Chapin III, F.S., 2004. Controls on moss evaporation in a boreal black spruce forest. Global Biogeochem. Cycles 18, GB2004. http://dx.doi.org/10.1029/2003GB002128.
Heikoop, J.M., Throckmorton, H.M., Newman, B.D., Perkins, G.B., Iversen, C.M., Roy Chowdhury, T., Romanovsky, V., Graham, D.E., Norby, R.J., Wilson, C.J., Wullschleger, S.D., 2015. Isotopic identification of soil and permafrost nitrate sources in an Arctic tundra ecosystem. J. Geophys. Res. Biogeosci. 120, 1000–1017. http://dx.doi.org/10.1002/2014JG002883.
Hinzman, L.D., Bettez, N.D., Bolton, W.R., Chapin, F.S., Dyurgerov, M.B., Fastie, C.L., Griffith, B., Hollister, R.D., Hope, A., Huntington, H.P., Jensen, A.M., Jia, G.J., Jorgenson, T., Kane, D.L., Klein, D.R., Kofinas, G., Lynch, A.H., Lloyd McGuire, A.H. A.D., Nelson, F.E., Oechel, W.C., Osterkamp, T.E., Racine, C.H., Romanovsky, V.E., Stone, R.S., Stow, D.A., Sturm, M., Tweedie, C.E., Vourlitis, G.L., Walker, M.D., Walker, D.A., Webber, P.J., Welker, J.M., Winker, K.S., Yoshikawa, K., 2005. Evidence and implications of recent climate change in Northern Alaska and other Arctic Regions. Clim. Change 72, 251–298. http://dx.doi.org/10.1007/s10584-005-5352-2.
Hinzman, L.D., Deal, C.J., McGuire, A.D., Mernild, S.H., Polyakov, I.V., Walsh, J.E., 2013. Trajectory of the Arctic as an integrated system. Ecol. Appl. 23 (8), 1837–1868.
Hsieh, C.-I., Katul, G., Chi, T., 2000. An approximate analytical model for footprint estimation of scalar fluxes in thermally stratified atmospheric flows. Adv. Water Resour. 23, 765–772. http://dx.doi.org/10.1016/S0309-1708(99)00042-1.
Hubbard, S.S., Gangodagamage, C., Dafflon, B., Wainwright, H., Peterson, J., Gusmeroli, A., Ulrich, C., Wu, Y., Wilson, C., Rowland, J., Tweedie, C., Wullschleger, S.D., 2013. Quantifying and relating land-surface and subsurface variability in permafrost environments using LiDAR and surface geophysical datasets. Hydrogeol. J. 21, 149–169. http://dx.doi.org/10.1007/s10040-012-0939-y.
Jorgenson, M.T., Shur, Y.L., Pullman, E.R., 2006. Abrupt increase in permafrost degradation in Arctic Alaska. Geophys. Res. Lett. 33, L02503. http://dx.doi.org/10.1029/2005GL024960.
Kane, D.L., Gieck, R.E., Hinzman, L.D., 1990. Evapotranspiration from a Small Alaskan Arctic watershed. Hydrol. Res. 21, 253–272.
Koch, J.C., Gurney, K., Wipfli, M.S., 2014. Morphology-dependent water budgets and nutrient fluxes in arctic thaw ponds. Permafrost Periglacial Proc. 25, 79–93. http://dx.doi.org/10.1002/ppp.1804.
Langford, Z., Kumar, J., Hoffman, F.M., Norby, R.J., Wullschleger, S.D., Sloan, V.L., Iversen, C.M., 2016. Mapping Arctic plant functional type distributions in the barrow environmental observatory using WorldView-2 and LiDAR datasets. Remote Sens. 8 (9), 733. http://dx.doi.org/10.3390/rs8090733.
Lara, M.J., McGuire, A.D., Euskirchen, E.S., Tweedie, C.E., Hinkel, K.M., Skurikhin, A.N., Romanovsky, V.E., Grosse, G., Bolton, W.R., Genet, H., 2015. Polygonal tundra geomorphological change in response to warming alters future CO_2 and CH_4 flux on the Barrow Peninsula. Glob. Change Biol. 21, 1634–1651. http://dx.doi.org/10.1111/gcb.12757.
Liljedahl, A.K., Hinzman, L.D., Harazono, Y., Zona, D., Tweedie, C.E., Hollister, R.D., Engstrom, R., Oechel, W.C., 2011. Nonlinear controls on evapotranspiration in arctic coastal wetlands. Biogeosciences 8, 3375–3389. http://dx.doi.org/10.5194/bg-8-3375-2011.
Liljedahl, A.K., Boike, J., Daanen, R.P., Fedorov, A.N., Frost, G.V., Grosse, G., Hinzman, L.D., Iijma, Y., Jorgenson, J.C., Matveyeva, N., Necsoiu, M., Raynolds, M.K., Romanovsky, V.E., Schulla, J., Tape, K.D., Walker, D.A., Wilson, C.J., Yabuki, H., Zona, D., 2016. Pan-Arctic ice-wedge degradation in warming permafrost and its influence on tundra hydrology. Nat. Geosci. 9, 312–318. http://dx.doi.org/10.1038/ngeo2674.
Mather, J.R., Thornthwaite, C.W., 1958. Microclimatic investigations at Point Barrow, Alaska, 1957–1958. Drexel Institute of Technology, Laboratory of Climatology – Meteorology 239 pages.
McVicar, T.R., Roderick, M.L., Donohue, R.J., Li, L.T., Van Niel, T.G., Thomas, A., Grieser, J., Jhajharia, D., Himri, Y., Mahowald, N.M., Mescherskaya, A.V., Kruger, A.C., Rehman, S., Dinpashoh, Y., 2012. Global review and synthesis of trends in observed terrestrial near-surface wind speeds: implications for evaporation. J. Hydrol. 416–417, 182–205. ISSN 0022-1694.
Mendez, J., Hinzman, L.D., Kane, D.L., 1998. Evapotranspiration from a wetland complex on the Arctic coastal plain of Alaska. Hydrol. Res. 29 (4–5), 303–330.
Newman, B.D., Throckmorton, H.M., Graham, D.E., Gu, B., Hubbard, S.S., Liang, L., Wu, Y., Heikoop, J.M., Herndon, E.M., Phelps, T.J., Wilson, C.J., Wullschleger, S.D., 2015. Microtopographic and depth controls on active layer chemistry in Arctic polygonal ground. Geophys. Res. Lett. 42, 1808–1817. http://dx.doi.org/10.1002/2014GL062804.
Nosko, P., Courtin, G.M., 1995. The water relations of Carex stans in wet sedge-moss tundra at a High Arctic oasis, Devon Island, NWT, Canada. Arctic Alpine Res., 137–145
Oechel, W.C., Van Cleve, K., 1986. The role of bryophytes in nutrient cycling in the taiga. In: Van Cleve, K. (Ed.), Forest Ecosystems in the Alaskan Taiga. Springer-Verlag, New York, pp. 121–137.
Pearson, R.G., Phillips, S.J., Loranty, M.M., et al., 2013. Shifts in Arctic vegetation and associated feedbacks under climate change. Nat. Clim. Change 3, 673–677. http://dx.doi.org/10.1038/nclimate1858.
Raz-Yaseef, N., Rotenberg, E., Yakir, D., 2010. Effects of spatial variations in soil evaporation caused by tree shading on water flux partitioning in a semi-arid pine forest. Agric. For. Meteorol. 150, 454–462. http://dx.doi.org/10.1016/j.agrformet.2010.01.010.
Raz-Yaseef, N., Torn, M.S., Wu, Y., Billesbach, D.P., Liljedahl, A.K., Kneafsey, T.J., Romanovsky, V.E., Cook, D.R., Wullschleger, S.D., 2016. Large CO_2 and CH_4 emissions from polygonal tundra during spring thaw in northern Alaska. Geophys. Res. Lett. 43. http://dx.doi.org/10.1002/2016GL071220.
Reichstein, M. et al., 2005. On the separation of net ecosystem exchange into assimilation and ecosystem respiration: review and improved algorithm. Glob. Change Biol. 11 (9), 1424–1439. http://dx.doi.org/10.1111/j.1365-2486.2005.001002.x.
Schlesinger, W.H., Bernhardt, E.S., 2013. Biogeochemistry : an analysis of global change.
Schädel, C., Bader, M.K.-F., Schuur, E.A.G., Biasi, C., Bracho, R., Čapek, P., De Baets, S., áková řina, Ernakovich, J., Estop-Aragones, C., Graham, D.E., Hartley, I.P., Iversen, C.M., Kane, E., Knoblauch, C., Lupascu, M., Martikainen, P.J., Natali, S.M., Norby, R.J., Donnell, A'., TRoy, Chowdhury, Šantrucková, H., Shaver, G., Sloan, L., Treat, C. C., Turetsky, M.R., Waldrop, M.P., Wickland, K.P., 2016. Potential carbon emissions dominated by carbon dioxide from thawed permafrost soils. Nat. Clim. Change 6, 950–953. http://dx.doi.org/10.1038/nclimate3054.
Schuur, E.A.G., Bockheim, J., Canadell, J.G., et al., 2008. Vulnerability of permafrost carbon to climate change: implications for the global carbon cycle. BioScience 58, 701–714.
Schuur, E.A.G. et al., 2015. Climate change and the permafrost carbon feedback. Nature 520, 171–179. http://dx.doi.org/10.1038/nature14338.
Screen, J.A., Francis, J.A., 2016. Contribution of sea-ice loss to Arctic amplification is regulated by Pacific Ocean decadal variability. Nat. Clim. Change 6, 856–860.
Spielhagen, R.F., Werner, K., Sørensen, S.A., Zamelczyk, K., Kandiano, E., Budeus, G., Husum, K., Marchitto, T.M., Hald, M., 2011. Enhanced modern heat transfer to the Arctic by warm Atlantic Water. Science 331, 450–453. http://dx.doi.org/10.1126/science.1197397.
Stoy, P.C., Street, L.E., Johnson, A.V., Prieto-Blanco, A., Ewing, S.A., 2012. Temperature, heat flux, and reflectance of common subarctic mosses and lichens under field conditions: might changes to community composition impact climate-relevent surface fluxes? Arct. Antarct. Alp. Res. 44, 500–508. http://dx.doi.org/10.1657/1938-4246-44.4.500.
Strauss, J., Schirrmeister, L., Grosse, G., Wetterich, S., Ulrich, M., Herzschuh, U., Hubberten, H.W., 2013. The deep permafrost carbon pool of the Yedoma region in Siberia and Alaska. Geophys. Res. Lett. 40 (23), 6165–6170.
Stuart, L., Oberbauer, S., Miller, P.C., 1982. Evapotranspiration measurements in Eriophorum vaginatum tussock tundra in Alaska. Ecography (Cop.) 5, 145–149. http://dx.doi.org/10.1111/j.1600-0587.1982.tb01029.x.
Sturtevant, C.S., Oechel, W.C., 2013. Spatial variation in landscape-level CO_2 and CH_4 fluxes from arctic coastal tundra: influence from vegetation, wetness, and the thaw lake cycle. Glob. Change Biol. 19, 2853–2866. http://dx.doi.org/10.1111/gcb.12247.
Swann, A.L., Fung, I.Y., Levis, S., Bonan, G.B., Doney, S.C., 2010. Changes in Arctic vegetation amplify high-latitude warming through the greenhouse effect. Proc. Natl. Acad. Sci. 107 (4), 1295–1300.
Tape, K., Sturm, M., Racine, C., 2006. The evidence for shrub expansion in Northern Alaska and the Pan-Arctic. Glob. Change Biol. 12, 686–702.
Throckmorton, H.M., Heikoop, J.M., Newman, B.D., Perkins, G.B., Feng, X., Graham, D. E., Wullschleger, S.D., Hinzman, L., Wilson, C.J., 2016. Stable Isotope Hydrology of Polygonal Ground in the Arctic Coastal Plain: Barrow, Alaska. Hydr. Proc. doi: 10.1002/hyp.10883.
Turetsky, M.R., Bond-Lamberty, B., Euskirchen, E., Talbot, J., Frolking, S., McGuire, A. D., Tuittila, E.S., 2012. The resilience and functional role of moss in boreal and arctic ecosystems. New Phytol. 196, 49–67. http://dx.doi.org/10.1111/j.1469-8137.2012.04254.x.

Villarreal, S., Hollister, R.D., Johnson, D.R., Lara, M.J., Webber, P.J., Tweedie, C.E., 2012. Tundra vegetation change near Barrow, Alaska (1972–2010). Environ. Res. Lett. 7 (1), 015508.

Wainwright, H.M., Dafflon, B., Smith, L.J., Hahn, M.S., Curtis, J.B., Wu, Y., Ulrich, C., Peterson, J.E., Torn, M.S., Hubbard, S.S., 2015. Identifying multiscale zonation and assessing the relative importance of polygon geomorphology on carbon fluxes in an Arctic tundra ecosystem. J. Geophys. Res. Biogeosci. 120, 788–808. http://dx.doi.org/10.1002/2014JG002799.

Wullschleger, S.D., Epstein, H.E., Box, E.O., Euskirchen, E.S., Goswami, S., Iversen, C. M., Kattge, J., Norby, R.J., van Bodegom, P.M., Xu, X., 2014. Plant functional types in Earth system models: past experiences and future directions for application of dynamic vegetation models in high-latitude ecosystems. Ann. Bot. 114, 1–16. http://dx.doi.org/10.1093/aob/mcu077.

Young-Robertson, J.M., Raz-Yaseef, N., Cohen, R.L., Newman, B., Rahn, T., Sloan, V., Wilson, C., Wullschleger, D.S., submitted for publication. Evaporation dominates evapotranspiration on Alaska's Arctic Coastal Plain.

Zhang, K., Kimball, J.S., Mu, Q., Jones, L.A., Goetz, S.J., Running, S.W., 2009. Satellite based analysis of northern ET trends and associated changes in the regional water balance from 1983 to 2005. J. Hydrol. 379, 92–110. http://dx.doi.org/10.1016/j.jhydrol.2009.09.047.